Dalton Transactions

Cite this: *Dalton Trans.*, 2012, **41**, 13741

www.rsc.org/dalton

PAPER

Magnetic variation induced by structural transformation from coordination chains to layers upon dehydration†

Xiao-Min Liu,[a] Bao-Ying Wang,[a] Wei Xue,[a] Lin-Hua Xie,[a] Wei-Xiong Zhang,[a] Xiao-Ning Cheng*[b] and Xiao-Ming Chen*[a]

Received 2nd July 2012, Accepted 2nd October 2012
DOI: 10.1039/c2dt31436c

The reaction of $CoBr_2$, 1,2-di(4*H*-1,2,4-triazol-4-yl)diazene (bta) and KSCN yielded a one-dimensional coordination polymer $[Co(SCN)_2(bta)(H_2O)_2]$ with water molecules coordinated to the metal ions. After dehydration at 100 °C, the compound transformed into a layered coordination polymer $[Co(SCN)_2(bta)]$, whose structure was determined by powder X-ray diffraction based on the single-crystal structure of another layered coordination polymer $[Cd(SCN)_2(bta)]$. Interestingly, a magnetic variation from a simple paramagnet to an antiferromagnetic ordered phase of a single-chain-magnet that exhibits both metamagnetic behaviour and slow magnetic relaxation was observed upon the dehydration process.

Introduction

In recent years, coordination polymers with solid-state structural transformations have become very attractive for their potential applications, such as separation, switches and sensors.[1–6] Many efforts have concentrated on the systematic modulation of magnetic behaviour as magnetic properties are sensitive to external stimuli, which is very helpful for studying the magneto-structural relationship. For example, Kepert and Kitagawa *et al.* have reported a number of flexible porous polymers induced by guest molecules.[7,8] Solid-state structural transformations with structural changes in the coordination dimensionality are abundant in this system,[9–15] including several metal thiocyanides and selenocyanates,[13,14] because the change in magnetic topology can induce acute diversification of the magnetic behaviour. Actually, the poor crystallinity presents a great challenge for structural characterizations of the transformed compounds and very few examples involving crystal-to-crystal transformations exhibiting drastic changes in the magnetic properties are known,[16–21] especially those transformations involving dimensionality changes of coordination polymers.[22–24]

As a continuing investigation towards our previous studies on the magneto–structural relationship through solid-state structural transformation,[25–28] we report herein a structure transformation from a one-dimensional (1D) coordination polymer $[Co(SCN)_2(bta)(H_2O)_2]$ (**1**) to a 2D coordination polymer $[Co(SCN)_2(bta)]$ (**2**), accompanyed with an interesting magnetic change from a simple paramagnet to an antiferromagnetic ordered phase of single-chain-magnets.

Experimental section

Materials and general methods

1,2-Di(4*H*-1,2,4-triazol-4-yl)diazene (bta) was prepared according to a literature method.[29] (**Caution!** Azo complexes are potentially explosive in the presence of organic compounds. Only a small amount of the material should be prepared and should be handled with care.) Anhydrous $CoBr_2$ (99%) was purchased from Sigma-Aldrich and all other reagents and solvents as AR grade were purchased from the Guangzhou Chemical Reagent Factory. All the chemicals were used as received without further purification.

ESI-MS spectra were measured on a SHIMADZU LCMS-2010A apparatus using an electrospray ionization source with MeOH as the mobile phase. Infrared spectra were recorded with a Bruker TENSOR 27 Fourier transform FT-IR spectrophotometer on KBr pellets in the range of 4000–400 cm^{-1}. Elemental (C, H, and N) analyses were performed on a Perkin-Elmer 240 elemental analyzer. Thermogravimetry (TG) analyses were performed on a Netzsch TG 209 instrument in flowing N_2 with a heating rate of 10 °C min^{-1}. Powder X-ray diffraction (PXRD) measurements were performed on a Bruker D8 ADVANCE X-ray diffractometer with Mo–Kα radiation. Magnetic susceptibility measurements of **1** and **2** were performed on poly-crystalline samples fixed with GE7031 varnish on a Quantum Design MPMS-XL7 SQUID. The data was corrected for both the background signal and diamagnetic contribution calculated from Pascal constants.

[a]*MOE Key Laboratory of Bioinorganic and Synthetic Chemistry, State Key Laboratory of Optoelectronic Materials and Technologies, School of Chemistry and Chemical Engineering, Sun Yat-Sen University, Guangzhou, 510275, P.R. China. E-mail: cxm@mail.sysu.edu.cn*
[b]*Instrumental Analysis and Research Center, Sun Yat-Sen University, Guangzhou, 510275, P.R. China. E-mail: chengxn7@mail.sysu.edu.cn*

†Electronic supplementary information (ESI) available: [DETAILS]. CCDC reference numbers 890531, 890532 and 901257. For ESI and crystallographic data in CIF or other electronic format see DOI: 10.1039/c2dt31436c

Synthesis

[Co(SCN)$_2$(bta)(H$_2$O)$_2$] (1). 1,2-Di(4*H*-1,2,4-triazol-4-yl)-diazene (bta) (0.205 g, 1.25 mmol) was first mixed with aqueous acetic acid (99.8%, 18 mL) (pH = 3–5) to form a solution suspension. The solution was heated to 95 °C for about 1 h to ensure the bta ligand was totally dissolved. $CoBr_2$ (0.271 g, 1.25 mmol) and KSCN (0.243 g, 2.5 mmol) were then added to this clarifying solution to react for 6 h at 95 °C. Finally, the pale-yellow solution was filtered off. Slow evaporation of the filtrate afforded red-brown crystals of **1** after 1 day. The mother liquid was decanted and the crystals were rinsed three times with H_2O (3 × 8 mL) and dried in air for several hours (yield: 0.421 g, *ca.* 90% based on Co). Anal. calcd (%) for $C_6H_8CoN_{10}O_2S_2$: C, 19.20; H, 2.15; N, 37.33. Found: C, 19.24; H, 2.05; N, 37.42. IR (cm^{-1}, KBr): 3338(w), 3125(w), 2093(s), 1664(m), 1496(s), 1384(m), 1324(w), 1183(s), 1053(s), 863(w), 700(m), 618(m), 550(w).

[Co(SCN)$_2$(bta)] (2). Heating **1** at 100 °C under vacuum gave microcrystalline **2**. Anal. calcd (%) for $C_6H_4N_{10}CoS_2$: C, 21.24; H, 1.19; N, 41.29. Found: C, 21.28 H, 1.16; N, 41.28. IR (cm^{-1}, KBr): 3122(w), 2121(s), 1705(w), 1494(s), 1381(m), 1309(w), 1218(s), 1040(s), 865(w), 696(m), 617(m), 551(w).

[Cd(SCN)$_2$(bta)] (3). A mixture of the bta ligand, acetic acid (HOAc, 99.8%) and water was heated and stirred to 120 °C for 1 h to form a uniform solution. $Cd(OAc)_2$ (0.290 g, 1.25 mmol) and KSCN (0.243 g, 2.5 mmol) were then slowly added into the above HOAc solution. The mixture was further stirred for another 5 h at 120 °C. Finally, the colourless solution was filtered off. Slow evaporation of the filtrate afforded colourless crystals of **3** after 1 week. The mother liquid was decanted and the crystals were rinsed three times with H_2O (3 × 8 mL) and dried in air for several hours (yield: 0.221 g, *ca.* 45% based on Cd). Anal. calcd (%) for $C_6H_4CdN_{10}S_2$: C, 18.35; H, 1.03; N, 35.67. Found: C, 18.27; H, 1.05; N, 35.60. IR (cm^{-1}, KBr): 3240(w), 1644(m), 1607(s), 1515(m), 1382(w), 1306(s), 1214(s), 1086(w), 1010(s), 817(m), 788(s), 667(w), 538(w).

Crystallography

The single-crystal diffraction data of **1** and **3** were collected on a Bruker Apex CCD area-detector diffractometer with Mo–Kα radiation. The structures were solved by direct methods and refined by the full-matrix least-squares method on F^2 using SHELXTL. All hydrogen atoms were placed geometrically and anisotropic thermal parameters were used to refine all non-hydrogen atoms. The crystal data and structure refinement results for these compounds are listed in Table 1.

The structure of **2** was determined by X-ray powder diffraction. The PXRD data of **2** was collected on a Bruker D8 Advance diffractometer with Cu–Kα X-ray (40 kV, 40 mA) at 293(2) K. Indexing, a Pawley refinement and Rietveld refinements of the PXRD pattern of **2** were carried out using a Reflex module of Material Studio.[30–32] The structure of **3** was used as the initial model for the Rietveld refinements. The crystallographic data and refinement results for **2** are listed in the ESI.†

Table 1 Crystallographic data and refinement parameters for **1**, **2** and **3**

	1	**2**	**3**
Empirical formula	$C_6H_8CoN_{10}O_2S_2$	$C_6H_4CoN_{10}S_2$	$C_6H_4CdN_{10}S_2$
Formula weight	375.27	339.21	392.71
Crystal system	Triclinic	Triclinic	Triclinic
Space group	$P\bar{1}$	$P\bar{1}$	$P\bar{1}$
T (K)	293(2)	293(2)	123(2)
a (Å)	6.071(3)	5.635(4)	5.849(2)
b (Å)	6.917(3)	6.908(5)	6.931(2)
c (Å)	9.026(4)	8.225(6)	8.268(2)
α (°)	84.037(6)	102.247(3)	106.923(3)
β (°)	81.307(5)	98.237(6)	96.000(3)
γ (°)	70.132(5)	104.470(5)	98.006(3)
V (Å^3)	351.8(3)	296.4(4)	313.9(2)
Z	1	1	1
D_c (g cm^{-3})	1.771	1.783	2.078
μ (mm^{-1})	1.538	—	2.075
No. of reflections collected	2697	—	1919
No. of unique reflections	1362	—	1209
R_{int}	0.0152	—	0.0117
Goodness of fit on F^2	1.007	—	1.006
R_1[a] [$I > 2\sigma(I)$]	0.0292	—	0.0165
wR_2[b] (all data)	0.0961	—	0.0440
R_p[c]	—	0.89%	—
R_{wp}[d]	—	1.28%	—
$\Delta\rho_{max}/\Delta\rho_{min}$ (e Å^{-3})	0.357/−0.579	—	0.401/−0.429

[a] $R_1 = \sum||F_o| - |F_c||/\sum|F_o|$. [b] $wR_2 = [\sum w(F_o^2 - F_c^2)^2/\sum w(F_o^2)^2]^{1/2}$, and $w = (\sigma^2(F_o^2)^2 + \{0.1[\max(0, F_o^2) + 2F_c^2]/3\}^2)^{-1}$. [c] $R_p = \Sigma|cY^{sim}(2\theta_i) - I^{exp}(2\theta_i) + Y^{back}(2\theta_i)|/\Sigma|I^{exp}(2\theta_i)|$. [d] $R_{wp} = \{w[cY^{sim}(2\theta_i) - I^{exp}(2\theta_i) + Y^{back}(2\theta_i)]^2/\Sigma w[I^{exp}(2\theta_i)]^2\}^{1/2}$, and $w = 1/I^{exp}(2\theta_i)$.

Results and discussion

Synthesis and crystal structures

The bta ligand has poor solubility in water and it has not been used for the synthesis of coordination polymers. We found that the addition of a small amount acetic acid into the mixture of $CoBr_2$, KSCN and bta (bta = 1,2-di(4*H*-1,2,4-triazol-4-yl)-diazene) can significantly increase the solubility, leading to the formation of reddish-brown crystals of [Co(SCN)$_2$(bta)(H$_2$O)$_2$] (**1**).

X-ray crystallographic analyses revealed that **1** crystallizes in the triclinic space group $P\bar{1}$. There is half a Co^{2+} ion, half a bta ligand, one water molecule and one SCN^- ion in the asymmetric unit of **1** (Fig. S1, ESI†). Each Co^{2+} ion in **1** is six-coordinate with two O atoms [Co–O 2.094(1) Å] from two coordinated H_2O molecules and four N atoms [Co–N 2.100(2)–2.172(3) Å] from two bta ligands and two SCN^- ions in a distorted octahedral geometry (Fig. 1a). Each bta ligand bridges two Co^{2+} ions in monodentate fashion *via* its two N atoms from the triazole rings, resulting in a chain structure (Fig. 1b). The water molecules and SCN^- ions are coordinated with the Co^{2+} ions of the chain as terminal ligands. The uncoordinated triazole N atoms and S atoms on the SCN^- ions form hydrogen bonds with the H_2O molecules on neighbouring chains (O–H···N 2.835(2) Å, O–H···S 3.233(2) Å, Fig. 1c). The hydrogen bonding interactions of the chains lead to 2D square-grid layers, which are

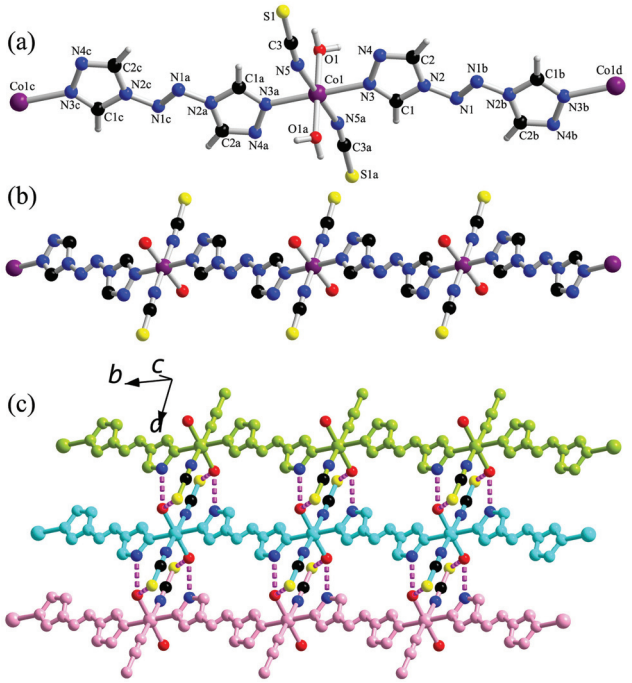

Fig. 1 Perspective views of (a) the coordination environment of Co1, (b) the structure of the 1D chain and (c) the stacking fashion of the 1D chains (the pink dotted lines represent the interchain hydrogen-bonding interactions) for **1**. Symmetry codes: $a = -x, 1 - y, 1 - z$; $b = -x, 2 - y, 2 - z$; $c = x, -1 + y, -1 + z$; $d = x, 1 + y, 1 + z$.

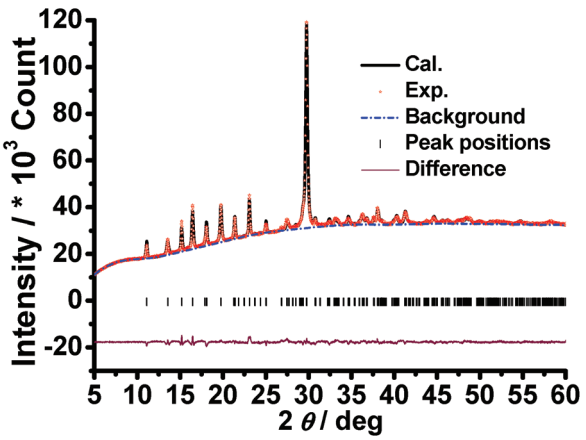

Fig. 2 The final Rietveld refinement plots of **2**.

further stacked into the 3D supramolecular structure of **1** *via* van der Waals forces (Table S1, ESI†).

It was noted that each S atom in the chain is very close to one Co atom in the adjacent chain [Co···S 4.581(2) Å] and Co···S bonds may be formed if the coordinated water molecules of **1** are removed. Thus thermogravimetric analysis (TGA) and powder X-ray diffraction (PXRD) were used to testify to the possible structure transformation (Fig. S7 and S9, ESI†). The TGA showed that **1** did release two H_2O molecules per formula unit (observed 14.0%, calc. 13.6%) below 100 °C. Subsequently, there is a long plateau until the decomposition around 310 °C. The dehydrated sample of **1** (after heating at 100 °C) displays a

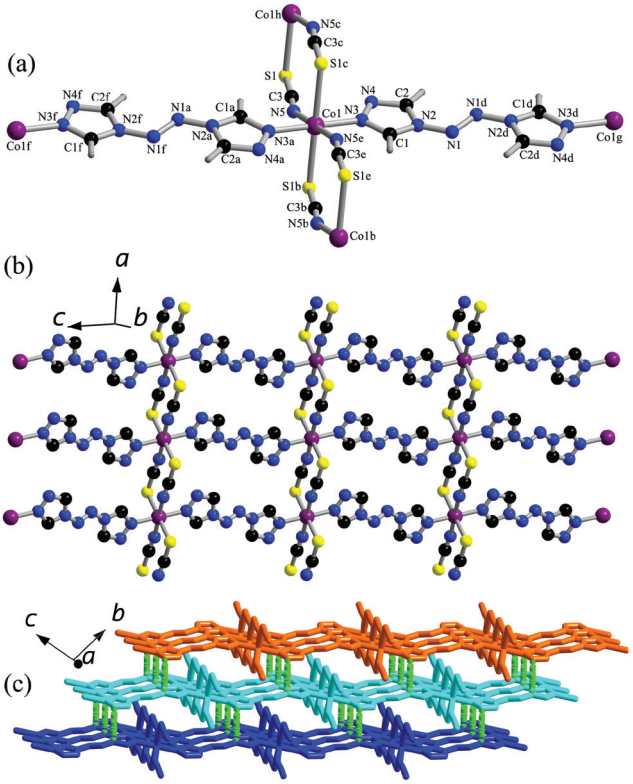

Fig. 3 Perspective views of (a) the coordination environment of the Co1 ion, (b) the structure of the 2D layer and (c) the stacking fashion of the 2D layers (the green dotted lines represent the interlayer π–π stacking interactions) for **2**. Symmetry codes: $a = 1 - x, 1 - y, -z$; $b = 1 + x, y, z$; $c = -x, 1 - y, -z$; $d = 1 - x, -y, 1 - z$; $e = 1 - x, 1 - y, -z$; $f = x, 1 + y, -1 + z$; $g = x, -1 + y, 1 + z$; $h = -1 + x, y, z$.

new PXRD pattern (Fig. 2 and Fig. S5, ESI†), indicating the formation of a new phase (denoted as **2**). The structure of **2** was quite stable in air and could not be changed back to the structure of **1** even though a sample of **2** was exposed to saturated water vapour for months.

Although some effort was made through single-crystal to single-crystal-solid transformations, we failed to obtain a large single crystal of **2**. We also could not obtain single crystals of **2** through a direct synthesis by a conventional solution method. Fortunately, in our attempt to synthesize other similar coordination polymers, single crystals of an isomorphic compound $[Cd(SCN)_2(bta)]$ (**3**) exhibiting a similar PXRD pattern with **2** were obtained.

The crystal structure of **3** can be conveniently solved by single-crystal diffraction. By taking the structure of **3** as the initial structural model, Rietveld refinements of the PXRD pattern of **2** gave a nice convergence, thus furnishing the precise structure of **2** (Fig. 3).

2 crystallizes in the triclinic space group $P\bar{1}$. There is half a Co^{2+} ion, half a bta ligand and half a thiocyanide ion in the asymmetric unit of **2** (Fig. S2, ESI†). Each Co^{2+} ion in **2** is six-coordinate with two S atoms [Co–S 2.595(1) Å] from two SCN^- ions and four N atoms [Co–N 2.052(1)–2.171(1) Å] from two triazole N atoms of two bta ligands and two N atoms of two SCN^- ions in a distorted octahedral geometry (Fig. 3a). Each pair of SCN^- ions and each bta ligand bridge two Co^{2+} ions,

respectively. The interconnection of the Co^{2+} ions by SCN^- ions and bta ligands results in a square-planar layer (Fig. 3b). Such layers stack *via* π–π interactions between interlayer triazole rings (3.47 Å) and interlayer van der Waals forces to form the 3D supramolecular structure of **2** (Fig. 3c and Table S1, ESI†). The coordination modes of the metal ions, bta ligands and SCN^- ions in **2** are the same as those in **3** (Fig. 4) due to the larger radius of the Cd^{2+} ion to the Co^{2+} ion. The bonds between the metal atoms and N atoms [2.264(2)–2.373(2) Å] or S atoms [2.728(1) Å] in **3** are longer than those in **2** (Table 2). Accordingly, the unit-cell volume of **3** (314 $Å^3$) is also larger than that of **2** (296 $Å^3$).

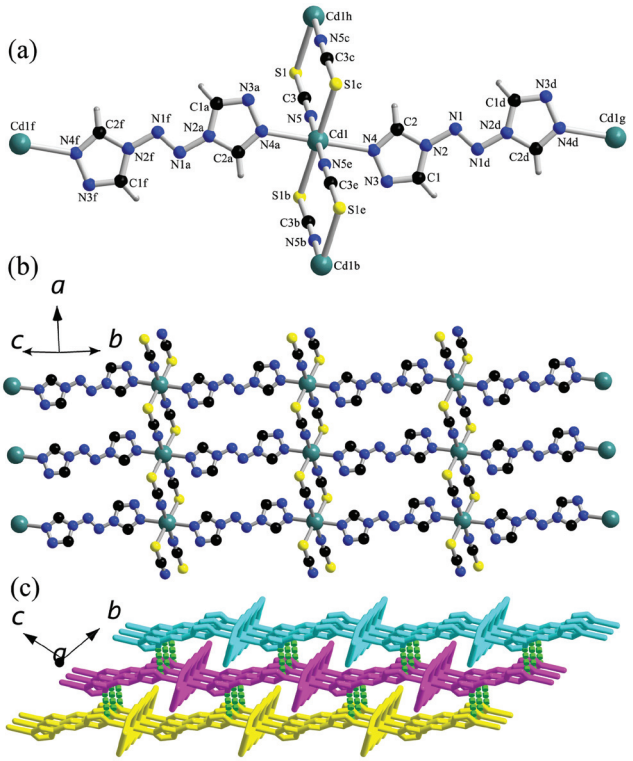

Fig. 4 Perspective views of (a) the coordination environment of the Cd1 ion, (b) the structure of the 2D layer and (c) the stacking fashion of the 2D layers (green dotted lines represent the interlayer π–π stacking interactions) for **3**. Symmetry codes: $a = 1 - x, 1 - y, -z$; $b = 1 + x, y, z$; $c = -x, 1 - y, -z$; $d = x, -1 + y, 1 + z$; $e = 1 - x, 1 - y, -z$; $f = x, 1 + y, -1 + z$; $g = x, -1 + y, 1 + z$; $h = -1 + x, y, z$.

It should be mentioned that, a related compound of **1** [$Co(SCN)_2(bpe)_2(H_2O)_2$], where 1,2-bis(4-pyridyl)ethylene (bpe) acts as a monodentate ligand, was reported by Näther *et al.* recently.[14] In this mononuclear compound, the monodentate bpe ligands are involved in hydrogen-bonding interactions. Thus, two steps are necessary for the structural transformation into the 2D layer compound $[Co(SCN)_2(bpe)]_n$, an analogue of **2**, and the second step, losing one bpe molecule, requires a higher temperature (*ca.* 300 °C). In contrast, only one step, losing H_2O molecules below 100 °C, is required in our case, which is achieved by the supramolecular design that each 1,2,4-triazole moiety of the bta ligand is involved in both coordination and hydrogen-bonding interactions.

Magnetic properties

The temperature-dependent magnetic susceptibility was measured for a fixed randomly-oriented polycrystalline sample of **1** in an applied dc field of 1 kOe. As shown in Fig. 5, the χT value of **1** is 2.97 $cm^3\ mol^{-1}\ K$ at 300 K, which is larger than the expected spin-only value (1.875 $cm^3\ K\ mol^{-1}$) for a high-spin octahedral Co^{2+} ion, indicating the orbit moment of the Co^{2+} ion is not quenched. Upon cooling, the χT value of **1** decreases slowly and reaches 0.97 $cm^3\ K\ mol^{-1}$ at 2.0 K, which is mostly caused by the single-ion anisotropy of the Co^{2+} ions. In addition, no significant signal in the ac susceptibility data has

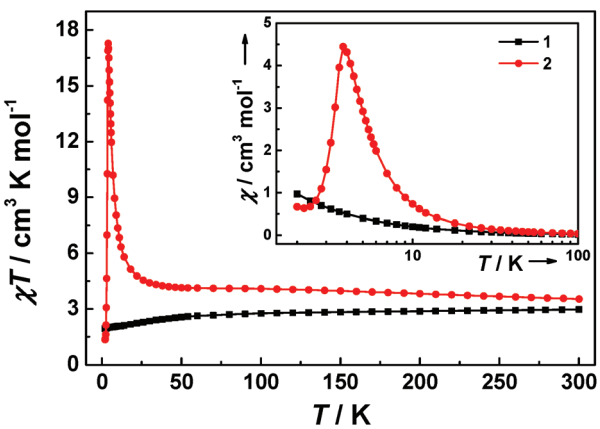

Fig. 5 The temperature-dependent susceptibility of **1** (●) and **2** (■), the solid line is a guide.

Table 2 Selected bond lengths (Å) and bond angles (°) for the complexes

1		**2**		**3**	
Co1–N3	2.094(1)	Co1–N3	2.052(1)	Cd1–N4	2.373(2)
Co1–N5	2.100(2)	Co1–N5	2.171(1)	Cd1–N5	2.264(2)
Co1–O1	2.171(1)	Co1–S1d	2.595(1)	Cd1–S1d	2.728(1)
N5–Co1–O1a	90.69(7)	N5–Co1–S1b	84.02(1)	N5–Cd1–S1b	86.57(5)
N5–Co1–N3	93.02(6)	N5–Co1–N3	84.89(2)	N5–Cd1–N4	91.65(7)
O1–Co1–N3	87.57(6)	N3–Co1–S1c	88.77(1)	N4–Cd1–S1c	87.73(4)
N5–Co1–N3a	86.98(6)	N5–Co1–N3a	95.11(2)	N5–Cd1–N4a	88.35(7)
N3–Co1–O1a	92.43(6)	N3–Co1–S1b	91.23(2)	N4–Cd1–S1b	92.27(4)
N5–Co1–O1	89.31(7)	N5–Co1–S1c	95.98(1)	N5–Cd1–S1c	93.43(5)

Symmetry codes: **1**: $a = -x, 1 - y, 1 - z$. **2**: $a = 1 - x, 1 - y, -z$; $b = 1 + x, y, z$; $c = -x, 1 - y, -z$; **3**: $a = 1 - x, 1 - y, -z$; $b = 1 + x, y, z$; $c = -x, 1 - y, -z$.

been observed for **1** down to 2.0 K (Fig. S10, ESI†). These facts indicate **1** is an ordinary paramagnet.

The magnetic property of **2** is distinctly different to **1** owing to the formation of the ditopic SCN^- bridges. The temperature dependence of the magnetic susceptibility for **2** in an applied field of 100 Oe is shown in Fig. 5. The χT value at 300 K is 3.53 cm^3 K mol^{-1}, which is larger than that of **1**, implying that the magnetic contribution from the orbit moment becomes larger in **2** after replacing coordinated O atoms by S atoms at the axial position of the Co^{2+} ion. After lowering the temperature, the χT value slightly increases to 4.4 cm^3 K mol^{-1} at 30 K, then increases rapidly to reach a maximum of 17.3 cm^3 K mol^{-1} at 4 K, indicating the intrachain ferromagnetic coupling between Co^{2+} ions. The rapid decrease of the χT value on further lowering T implys that antiferromagnetic ordering is formed by interchain antiferromagnetic interactions. This antiferromagnetic ordering is further confirmed by a sharp peak found at 3.8 K in the χ *vs.* T plot (inset of Fig. 4). Since the single-ion anisotropy of Co^{2+} is relatively strong in **2**, the susceptibility data obtained on a single-crystal sample is necessary for estimating both the 1D intrachain interactions and the single-ion anisotropy. Unfortunately, it is unavailable at present because **2** was obtained as a powder sample.

The magnetization curve at 1.8 K reveals an *S*-shaped curve in the low field region and then rapidly increases to 1.7 Nβ at 5.5 kOe, indicating a transition from antiferromagnetic ordering to a paramagnetic phase. The magnetization is not fully saturated at 70 kOe (2.2 Nβ), implying a strong magnetic anisotropy in **2**. The extrapolation (H_a) of magnetization is 275 kOe at the expected saturation value, which is assumed to be 3.3 Nβ if taking a typical average g factor of 2.2 for the Co^{2+} ion ($S = 3/2$) (Fig. S11, ESI†). Thus, a phenomenological anisotropy energy, K_A/k_B, where k_B is the Boltzmann constant, is estimated at about 30 K by $2K_A = gS\mu_B H_a$.[33] In order to classify the field-induced metamagnetic transition for **2**, field-cooling magnetizations in various dc fields and field-dependent magnetizations at various temperatures were measured. A corresponding phase diagram was proposed for **2**, shown in the inset of Fig. 6, indicating an antiferromagnetically ordered ground state is formed below the Neel temperature of 3.8 K in a zero dc field and is suppressed by an applied field of *ca.* 1350 Oe.

Moreover, below *ca.* 2.5 K, an increase in the magnetization was observed in both the zero-field-cooling and field-cooling curves upon further lowering the temperature (Fig. S13, ESI†) and a slight frequency-dependence on the ac magnetic susceptibilities in a zero dc field was also observed below 2.6 K (Fig. 7a), implying a slow magnetic relaxation exists in **2**. This slow-relaxing dynamic was further confirmed by the ac magnetic susceptibility data in an applied dc field of 1500 Oe, which was strong enough to overwhelm the interchain antiferromagnetic interactions. As shown in Fig. 7b, the sharp peak of χ' at 3.9 K completely disappeared while the frequency-dependency of both χ' and χ'' at lower temperature was enhanced. The shift of the peak temperature (T_p) of χ'' at different ac frequencies (f) was measured by $\psi = (\Delta T_p/T_p)/\Delta\log(2\pi f) = 0.1$, which was larger than those of canonical spin glasses.[34] Furthermore, the temperature-dependent relaxation time $\tau(T)$ follows a thermally activated law: $\tau(T) = \tau_0 \exp(U/k_B T)$, with an energy barrier of $U/k_B = 52$ K and a prefactor of $\tau_0 = 1.6 \times 10^{-13}$ s, which is similar to the analogues reported by Näther *et al.*[13,14] For a uniform ferromagnetic chain, the static magnetic susceptibility at low temperature is directly related to the correlation length ξ, suggesting an exponential divergence of χT with T: $\chi T \propto \exp(\Delta_\xi/k_B T)$, where the slope, Δ_ξ/k_B, obtained from a linear analysis of $\ln(\chi T)$ *vs.* T^{-1} is directly related to the exchange contribution for a SCM.[35]

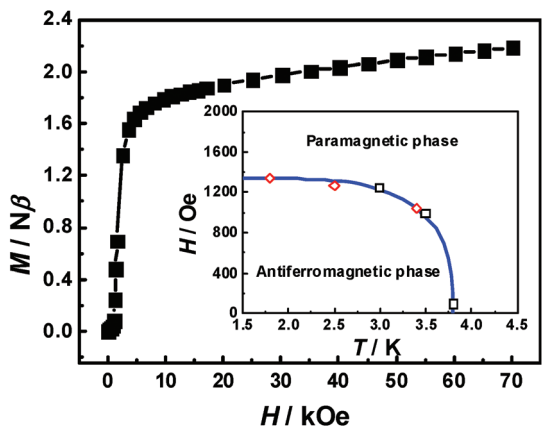

Fig. 6 The isothermal magnetization for **2** at 1.8 K. Inset: phase diagram proposed for **2** from the location of the maximum of dM/dH *vs.* H (◇) and dM/dH *vs.* T (□).

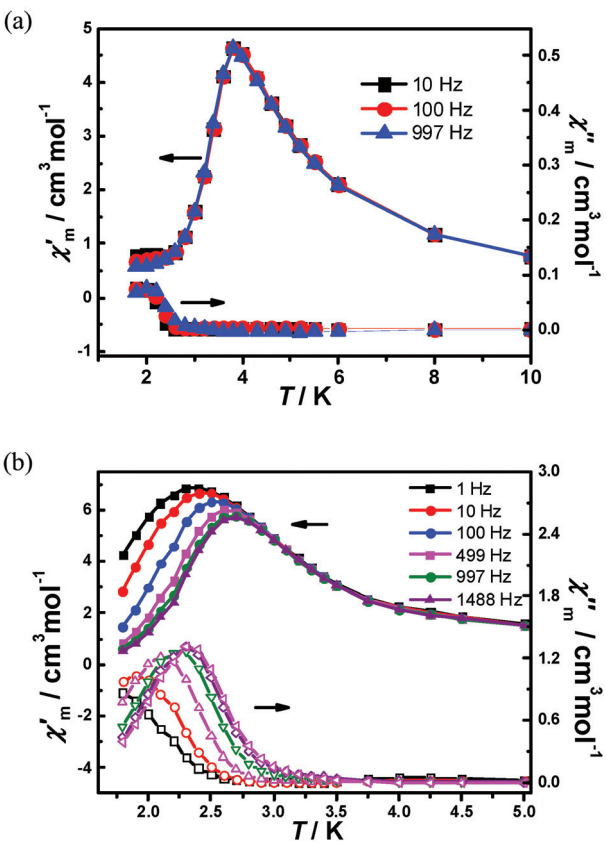

Fig. 7 Temperature dependent ac magnetic susceptibility of **2**, obtained at the indicated frequencies in zero dc field (a) and an applied dc field of 1500 Oe (b).

A linear analysis of $\ln(\chi T)$ *vs.* T^{-1} in the temperature region of 4.8–10.0 K (Fig. S13, ESI†) afforded a Δ_ξ value of 7.9 K for **2**. The corresponding intrachain exchange coupling parameter J is about 0.9 K, when taking $\Delta_\xi = 4JS^2$ ($S = 3/2$) and is slightly smaller than that observed in an analogue with SeCN-bridged Co(II) chains.[13] Taking into account the anisotropy energy K_A, a calculated energy barrier is obtained: $U_{cal}/k_B = (2\Delta_\xi + K_A)/k_B \approx 46$ K, which is close to the experimental value (52 K). Thus, the slow relaxation dynamics observed in an applied field for **2** is an intrinsic slow magnetic relaxation of a 1D chain,[35,36] mainly arising from the strong uniaxial anisotropy of the Co^{2+} ion and intrachain ferromagnetic interaction. In short, these facts indicate that **2** is a new magnet featuring an antiferromagnetic phase of single-chain magnets that exhibits both metamagnetic behaviour and slow magnetic relaxation.[33,37]

Conclusions

In summary, a unique solid-state structural transformation from a 1D single chain to a 2D layered coordination polymer has been established. Although single crystals of **2** can not be obtained, a PXRD method was utilized to determine the structure of the new phase, based on the single-crystal structure of a similar compound as the initial model. More interestingly, upon the dehydration process, an addition of magnetic exchange paths was observed from **1** to **2**, leading to a unique magnetism variation from a simple paramagnet to an antiferromagnetic ordered phase of single-chain-magnets.

Acknowledgements

This work was supported by the NSFC (90922031, 21121061 and 50902151), the "973 Project" (2012CB821706) and the Foundation for the Authors of Excellent Doctoral Dissertation of Guangdong Province.

Notes and references

1 L. E. Kreno, K. Leong, O. K. Farha, M. Allendorf, R. P. Van Duyne and J. T. Hupp, *Chem. Rev.*, 2012, **112**, 1105–1125.
2 J.-R. Li, J. Sculley and H.-C. Zhou, *Chem. Rev.*, 2012, **112**, 869–932.
3 J.-P. Zhang, Y.-B. Zhang, J.-B. Lin and X.-M. Chen, *Chem. Rev.*, 2012, **112**, 1001–1033.
4 N. Yanai, T. Uemura, M. Inoue, R. Matsuda, T. Fukushima, M. Tsujimoto, S. Isoda and S. Kitagawa, *J. Am. Chem. Soc.*, 2012, **134**, 4501–4504.
5 S. M. Cohen, *Chem. Rev.*, 2012, **112**, 970–1000.
6 M. C. Das, S. C. Xiang, Z. J. Zhang and B. L. Chen, *Angew. Chem., Int. Ed.*, 2011, **50**, 10510–10520.
7 G. J. Halder, C. J. Kepert, B. Moubaraki, K. S. Murray and J. D. Cashion, *Science*, 2002, **298**, 1762–1765.
8 S. K. Ghosh, W. Kaneko, D. Kiriya, M. Ohba and S. Kitagawa, *Angew. Chem., Int. Ed.*, 2008, **47**, 8843–8847.
9 Y. Yoshida, K. Inoue and M. Kurmoo, *Inorg. Chem.*, 2009, **48**, 10726–10736.
10 M.-H. Xie, X.-L. Yang and C.-D. Wu, *Chem.–Eur. J.*, 2011, **17**, 11424–11427.
11 L. Wen, P. Cheng and W. B. Lin, *Chem. Commun.*, 2012, **48**, 2846–2848.
12 P. Zhu, W. Gu, L.-Z. Zhang, X. Liu, J.-L. Tian and S.-P. Yan, *Eur. J. Inorg. Chem.*, 2008, 2971–2974.
13 S. Wöhlert, U. Ruschewitz and C. Näther, *Cryst. Growth Des.*, 2012, **12**, 2715–2718.
14 S. Wöhlert, J. Boeckmann, M. Wriedt and C. Näther, *Angew. Chem., Int. Ed.*, 2011, **50**, 6920–6923.
15 J. Boeckmann and C. Näther, *Dalton Trans.*, 2010, **39**, 11019–11026.
16 Y. Gong, J. Li, T. Wu, J. Qin, R. Cao and J. Li, *CrystEngComm*, 2012, **14**.
17 B. Zhang, D. Zhu and Y. Zhang, *Chem.–Asian J.*, 2011, **6**, 1367–1371.
18 W. Kaneko, M. Ohba and S. Kitagawa, *J. Am. Chem. Soc.*, 2007, **129**, 13706–13712.
19 S. K. Ghosh, J. P. Zhang and S. Kitagawa, *Angew. Chem., Int. Ed.*, 2007, **46**, 7965–7968.
20 L.-F. Ma, L.-Y. Wang, D.-H. Lu, S. R. Batten and J.-G. Wang, *Cryst. Growth Des.*, 2009, **9**, 1741–1749.
21 K. D. Demadis, M. Papadaki, M. A. G. Aranda, A. Cabeza, P. Olivera-Pastor and Y. Sanakis, *Cryst. Growth Des.*, 2009, **10**, 357–364.
22 Z. Duan, Y. Zhang, B. Zhang and D. Zhu, *J. Am. Chem. Soc.*, 2009, **131**, 6934–6935.
23 Y.-J. Zhang, T. Liu, S. Kanegawa and O. Sato, *J. Am. Chem. Soc.*, 2009, **131**, 7942–7943.
24 B. Zhang, D. Zhu and Y. Zhang, *Chem.–Eur. J.*, 2010, **16**, 9994–9997.
25 X.-N. Cheng, W.-X. Zhang and X.-M. Chen, *J. Am. Chem. Soc.*, 2007, **129**, 15738–15739.
26 W.-X. Zhang, W. Xue and X.-M. Chen, *Inorg. Chem.*, 2010, **50**, 309–316.
27 X. F. Wang, Y. Wang, Y. B. Zhang, W. Xue, J. P. Zhang and X. M. Chen, *Chem. Commun.*, 2012, **48**, 133–135.
28 J. P. Zhang, X. L. Qi, C. T. He, Y. Wang and X. M. Chen, *Chem. Commun.*, 2011, **47**, 4156–4158.
29 C. Qi, S. H. Li, Y. C. Li, Y. A. Wang, X. K. Chen and S. P. Pang, *J. Mater. Chem.*, 2011, **21**, 3221–3225.
30 G. S. Pawley, *J. Appl. Crystallogr.*, 1981, **14**, 357–361.
31 A. Boultif and D. Louer, *J. Appl. Crystallogr.*, 1991, **24**, 987–993.
32 *Materials Studio v5.5*, Accelrys Inc, San Diego, CA, 2010.
33 H. Miyasaka, K. Takayama, A. Saitoh, S. Furukawa, M. Yamashita and R. Clérac, *Chem.–Eur. J.*, 2010, **16**, 3656–3662.
34 J. A. Mydosh, *Spin Glasses: An Experimental Introduction*, Taylor & Francis, London, 1993.
35 C. Coulon, H. Miyasaka and R. Clérac, *Struct. Bonding*, 2006, **122**, 163–206.
36 L. Bogani, A. Vindigni, R. Sessoli and D. Gatteschi, *J. Mater. Chem.*, 2008, **18**, 4750–4758.
37 C. Coulon, R. Clérac, W. Wernsdorfer, T. Colin and H. Miyasaka, *Phys. Rev. Lett.*, 2009, **102**, 167204.

